Acta Crystallographica Section D
**Biological Crystallography**
ISSN 0907-4449

# Structure and implications for the thermal stability of phosphopantetheine adenylyltransferase from *Thermus thermophilus*

**Hitomi Takahashi,[a] Eiji Inagaki,[a] Yayoi Fujimoto,[a] Chizu Kuroishi,[a] Yuichi Nodake,[a] Yuki Nakamura,[a] Fumio Arisaka,[b] Katsuhide Yutani,[a] Seiki Kuramitsu,[c] Shigeyuki Yokoyama,[d] Masaki Yamamoto,[a,e] Masashi Miyano[a,f] and Tahir H. Tahirov[a]***

[a]Highthroughput Factory, RIKEN Harima Institute, 1-1-1 Kouto, Mikazuki-cho, Sayo-gun, Hyogo 679-5148, Japan, [b]Graduate School of Bioscience and Biotechnology, Tokyo Institute of Technology, 4529 Nagatsuta, Midori-ku, Yokohama 226-8501, Japan, [c]Department of Biology, Graduate School of Science, Osaka University, Toyonaka, Osaka 560, Japan, [d]Genomic Sciences Center, RIKEN Yokohama Institute, 1-7-22 Suehiro-cho, Tsurumi, Yokohama 230-0045, Japan, [e]Coherent X-Ray Optics Laboratory, RIKEN Harima Institute, 1-1-1 Kouto, Mikazuki-cho, Sayo-gun, Hyogo 679-5148, Japan, and [f]Structural Biophysics Laboratory, RIKEN Harima Institute, 1-1-1 Kouto, Mikazuki-cho, Sayo-gun, Hyogo 679-5148, Japan

Correspondence e-mail: tahir@spring8.or.jp



Received 13 August 2003
Accepted 3 November 2003

**PDB Reference:** 1od6, r1od6sf.

Phosphopantetheine adenylyltransferase (PPAT) is an essential enzyme in bacteria that catalyzes the rate-limiting step in coenzyme A (CoA) biosynthesis by transferring an adenylyl group from ATP to 4′-phosphopantetheine (Ppant), yielding 3′-dephospho-CoA (dPCoA). The crystal structure of PPAT from *Thermus thermophilus* HB8 (*Tt* PPAT) complexed with Ppant has been determined by the molecular-replacement method at 1.5 Å resolution. The overall fold of the enzyme is almost the same as that of *Escherichia coli* PPAT, a hexamer having point group 32. The asymmetric unit of *Tt* PPAT contains a monomer and the crystallographic triad and dyad coincide with the threefold and twofold axes of the hexamer, respectively. Most of the important atoms surrounding the active site in *E. coli* PPAT are conserved in *Tt* PPAT, indicating similarities in their substrate binding and enzymatic reaction. The notable difference between *E. coli* PPAT and *Tt* PPAT is the simultaneous substrate recognition by all six subunits of *Tt* PPAT compared with substrate recognition by only three subunits in *E. coli* PPAT. Comparative analysis also revealed that the higher stability of *Tt* PPAT arises from stabilization of each subunit by hydrophobic effects, hydrogen bonds and entropic effects.

## 1. Introduction

Coenzyme A (CoA) is the principal acyl carrier in all living systems and is widely required in synthetic and degradative metabolic pathways (Geerlof *et al.*, 1999). The five-step pathway for CoA biosynthesis from pantothenate (vitamin $B_5$), cysteine and ATP is common to all organisms (Robinshaw & Neely, 1985; Gerdes *et al.*, 2002). Phosphopantetheine adenylyltransferase (PPAT), a member of the nucleotidyltransferase superfamily (Bork *et al.*, 1995), catalyzes the penultimate step of the pathway: the reversible transfer of an adenylyl group from ATP to 4′-phosphopantetheine (Ppant), yielding dephospho-CoA (dPCoA) and pyrophosphate. The rate of CoA biosynthesis is regulated by feedback inhibition of the first enzyme of the pathway, pantothenate kinase (Halvorsen & Skrede, 1982). Studies of the CoA metabolic intermediates in *Escherichia coli* have revealed that both pantothenate and Ppant accumulate in the cell (Jackowski & Rock, 1984), suggesting that PPAT catalyzes an additional rate-limiting step in the pathway. PPAT is thus an attractive antibacterial target.

Crystal structures of *E. coli* PPAT have been reported in three binary complexes: with ATP, with Ppant and with its major product dPCoA (Izard, 2002; Izard & Geerlof, 1999). These structures have revealed the PPAT catalytic mechanism. The 4′-phosphate of Ppant undergoes nucleophilic attack on the $\alpha$-phosphate of ATP *via* an in-line displacement

mechanism. The enzyme promotes the reaction by orienting the nucleotide and stabilizing the pentacovalent transition state without involving its functional groups in a chemical sense. In particular, the conserved His18 of the sequence motif T*x*GH plays an essential role in transition-state stabilization (Izard, 2002).

We now report the crystal structure of PPAT from *Thermus thermophilus* HB8 (*Tt* PPAT; $M_r$ = 17 707) complexed with Ppant at 1.50 Å resolution. The thermostabilization mechanism is also discussed from the viewpoint of its crystal structure by comparing it with that of *E. coli* PPAT.

## 2. Materials and methods

### 2.1. Protein expression and purification

The gene was amplified by the polymerase chain reaction (PCR) using *T. thermophilus* HB8 genomic DNA as the template. The PCR product was ligated with pT7blue (Novagen). The plasmid was digested with *Nde*I and *Bgl*II and the fragment was inserted into the expression vector pET-11a linearized with *Nde*I and *Bam*HI. The recombinant plasmid was transformed into *E. coli* BL21 (DE3) cells and grown at 310 K in LB medium containing 50 µg ml$^{-1}$ ampicillin for 20 h. The cells were harvested by centrifugation at 6500 rev min$^{-1}$ for 5 min, suspended in 20 m*M* Tris–HCl pH 8.0 (buffer *A*) containing 0.5 *M* NaCl and 5 m*M* 2-mercaptoethanol and disrupted by sonication. The supernatant was heated at 343 K for 11.5 min. After heat treatment, the cell debris and denatured proteins were removed by centrifugation (14 000 rev min$^{-1}$ for 30 min) and the supernatant solution was used as the crude extract for purification. The crude extract was desalted using a HiPrep 26/10 desalting column (Amersham Biosciences) and applied onto a SuperQ Toyopearl 650M column (Tosoh) equilibrated with buffer *A*. The protein was eluted with a linear gradient of 0–0.3 *M* NaCl. The fraction containing the protein was desalted using a HiPrep 26/10 column with buffer *A* and subjected to a Resource Q column (Amersham Biosciences) equilibrated with buffer *A*. The protein was eluted with a linear gradient of 0–0.3 *M* NaCl. The fraction containing the protein was desalted using a HiPrep 26/10 column containing 10 m*M* phosphate pH 7.0 and applied onto a Bio-Scale CHT-20-I column (Bio-Rad) equilibrated with the same buffer. The protein was eluted with a linear gradient of 10–100 m*M* phosphate pH 7.0. The fractions containing the protein were pooled, concentrated by ultrafiltration (Amicon, 5 kDa cutoff) and loaded onto a HiLoad 16/60 Superdex 200 pg column (Amersham Biosciences) equilibrated with buffer *A* containing 0.2 *M* NaCl. The purified protein was homogeneous on SDS–PAGE.

### 2.2. Crystallization and data collection

Crystals of *Tt* PPAT complexed with Ppant were obtained at 291 K using the oil batch method by TERA (Sugahara & Miyano, 2002). A 0.5 µl aliquot of protein solution (4.13 mg ml$^{-1}$ protein, 20 m*M* Tris–HCl pH 8.0, 0.2 *M* NaCl) was mixed with an equal volume of reservoir solution (1.1 *M* $Li_2SO_4$, 0.1 *M* Na MES pH 6.25) and covered with 15 µl of paraffin oil. After two weeks, crystals had grown to full size (0.1 × 0.1 × 0.15 mm). The crystals belonged to space group *R*32, with a monomer in the asymmetric unit, a solvent content of 70% and a specific volume $V_M$ of 4.2 Å$^3$ Da$^{-1}$ (Matthews, 1968). For data collection, these crystals were flash-cooled in a 100 K dry nitrogen stream and 25% glycerol was used as the cryoprotectant. Data were collected at beamline 26B1, SPring-8, Harima, Japan. The data were processed using the programs *DENZO* and *SCALEPACK* (Otwinowski & Minor, 1997). The X-ray crystallographic data for *Tt* PPAT are summarized in Table 1.

**Table 1**
Data-collection and refinement statistics for *Tt* PPAT.

| | |
|---|---|
| Data collection† | |
| Wavelength (Å) | 1.00 |
| Data-collection temperature (K) | 100 |
| No. of crystals/images | 1/342 |
| Space group | *R*32 |
| Unit-cell parameters (Å) | $a = b = 115.92$, $c = 115.75$ |
| Resolution range (Å) | 50–1.50 (1.55–1.50) |
| Measured reflections | 334505 |
| Unique reflections | 47654 |
| $I/\sigma(I)$ | 23.6 |
| Completeness (%) | 99.3 (98.3) |
| $R_{merge}$ (%) | 4.0 (35.9) |
| Refinement | |
| $R_{cryst}$‡ (%)/$R_{free}$§ (%) | 19.62/20.05 |
| No. of molecules per asymmetric unit | 1 |
| No. of protein atoms | 1229 |
| No. of solvent molecules | 162 |
| No. of substrate (sulfate) molecules | 1 (3) |
| Average *B* factor (Å$^2$) | 26.2 |
| R.m.s.d. | |
| Bonds (Å) | 0.005 |
| Angles (°) | 1.1 |
| Dihedrals (°) | 21.7 |
| Impropers (°) | 0.72 |
| Coordinate error from (Å) | |
| Luzzati plot | 0.18 (0.19¶) |
| $\sigma_A$ plot (Å) | 0.22 (0.22¶) |
| Ramachandran plot, residues in (%) | |
| Favoured regions | 95.6 |
| Allowed regions | 4.4 |
| Generous regions | 0.0 |
| Disallowed regions | 0.0 |

† Values in parentheses are for the highest resolution shell. ‡ $R_{cryst}$ was calculated from the working set (95% of the data). § $R_{free}$ was calculated from the test set (5% of the data). ¶ Cross-validated value.

### 2.3. Structure determination and refinement

The structure was determined by the molecular-replacement method using the program *CNS* (Brünger *et al.*, 1998). Chain *A* of PPAT from *E. coli* complexed with Ppant (PDB code 1qjc) was used as the search model. Refinement was carried out using *CNS* (Brünger *et al.*, 1987). The structure was visualized and modified using the program *QUANTA* (Accelrys). The data-collection and refinement statistics are summarized in Table 1. The refined model consists of 1229 protein atoms, one Ppant ligand, three sulfate ions and 162 water molecules and showed a stereochemically reasonable structure (Table 1). Electron density was not observed for the flexible loop comprised of residues 38–42.

### 2.4. Analytical ultracentrifugation

Sedimentation-velocity and sedimentation-equilibrium measurements were carried out using a Beckman-Coulter XL-I with an An60 Ti rotor and double-sector cells at 293 and 277 K, respectively. Before taking measurements, the protein solution was dialyzed overnight against buffer *A* containing 0.2 *M* NaCl and the dialysate was used as the reference solution. The sedimentation-velocity experiment at a protein concentration of 1.38 mg ml$^{-1}$ was carried out at 50 000 rev min$^{-1}$. In the sedimentation equilibrium experiments, three different loading concentrations between 0.26 and 0.86 mg ml$^{-1}$ were used and the samples were sequentially run for 24 h at 7000 rev min$^{-1}$, 20 h at 9000 rev min$^{-1}$ and 20 h at 12 000 rev min$^{-1}$ so as to reach equilibrium at each speed of rotation. Attainment of equilibrium was judged by superposition of the last three scans; scans were taken every 2 h. Analysis of the sedimentation equilibrium was performed using the global fitting program supplied with the Beckman-Coulter XL-I and the sedimentation-velocity data were analyzed using *SVEDBERG*. The partial specific volume of 0.7487 cm$^3$ g$^{-1}$ used for *Tt* PPAT was based on the amino-acid composition of the protein. The partial specific volume, solvent viscosity and solvent density were calculated using the *SEDNTERP* program (*SVEDBERG* and *SEDNTERP* were kindly provided by Dr John Philo).

## 3. Results and discussion

### 3.1. Overall structure and homohexamer interaction of *Tt* PPAT

The structure was determined by the molecular-replacement method using the structure of *E. coli* PPAT as the search model (the primary sequence identity was 48%; Izard, 2002). The *Tt* PPAT molecule is a hexamer with point group 32. The overall shape of the molecule is spherical, with a diameter of 65 Å and a 13 Å wide hole which coincides with the molecule triad axis and enables the entry of ligands (Fig. 1). Each subunit of the molecule interacts with four neighbouring subunits. Two of these are subunits related to the triad axis and one is the subunit related to the dyad axis. The intersubunit interactions are most extensive across dyad axis of the oligomer and involve ten intersubunit hydrogen bonds. The dyad contacts involve 13 hydrophobic side chains. Dimerization results in a total buried surface area of 2000 Å$^2$ (2100 Å$^2$ in *E. coli* PPAT). The trimer contacts involve only two intersubunit hydrogen bonds. The protomer surfaces implicated in trimer formation bury a total of 3100 Å$^2$ of the solvent-accessible surface (3500 Å$^2$ in the Ppant-bound trimer of *E. coli* PPAT). The other intersubunit contact (between the blue and the red subunits in Fig. 1) involved no hydrogen bonds and the surface area buried at the interface is 490 Å$^2$. The asymmetric unit contains a monomer and the crystallographic triad and dyad coincide with the threefold and twofold axes of the hexamer, respectively.

### 3.2. Protomer structure of *Tt* PPAT

As shown in Fig. 2, the protomer of PPAT consists of a five-stranded parallel $\beta$-pleated sheet folded in the manner known as the dinucleotide-binding fold (or canonical Rossmann-binding fold; Rossmann *et al.*, 1975) and seven $\alpha$-helices. Residues 38–42 in the loop between $\beta$2 and $\alpha$2 appear to be disordered. The loop seems to be positioned near the mouth of the solvent channel that runs through the entire hexamer along its triad axis. Strong electron density corresponding to

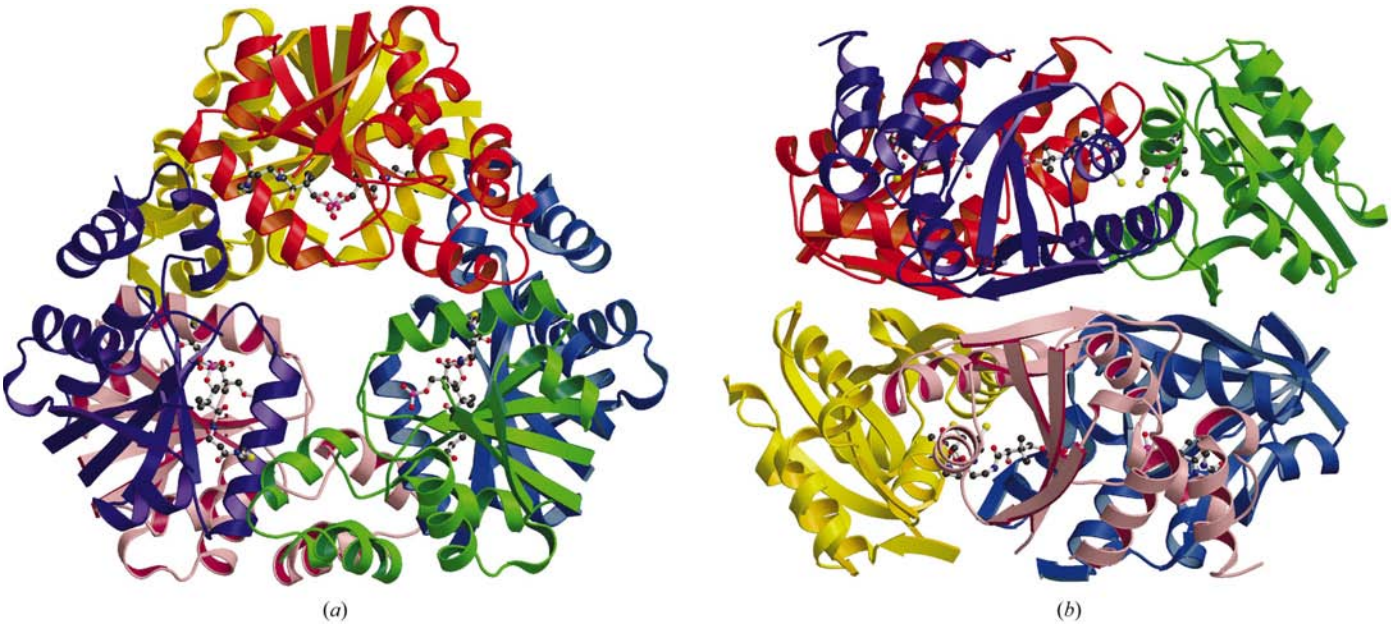


**Figure 1**
Overall structure of *Tt* PPAT with bound Ppant molecules. Each of the six subunits is coloured differently. Ppant molecules are shown in ball-and-stick representation. O atoms are red, N atoms blue, S atoms yellow, C atoms black and phosphates pink. (*a*) View down the triad axis. (*b*) View perpendicular to (*a*). This figure was produced with *MOLSCRIPT* and *Raster3D* (Kraulis, 1991; Merritt & Bacon, 1997).

the substrate Ppant was found in the active-site cleft of each protomer (Fig. 3). The fact that the Ppant was not released from the enzyme during the various steps of the purification protocol indicated that it was very tightly bound. The average temperature factor of the ligand refined to 31.3 Å$^2$ for full occupancy, which is similar to that of the protein (24.5 Å$^2$). In the *Tt* PPAT–Ppant crystal structure it appears that each subunit of the hexamer binds the ligand, while the *E. coli* PPAT–Ppant crystal structure, which contains a dimer in the asymmetric unit, revealed the hexamer to consist of two distinct trimers with only one trimer binding Ppant (Izard, 2002).

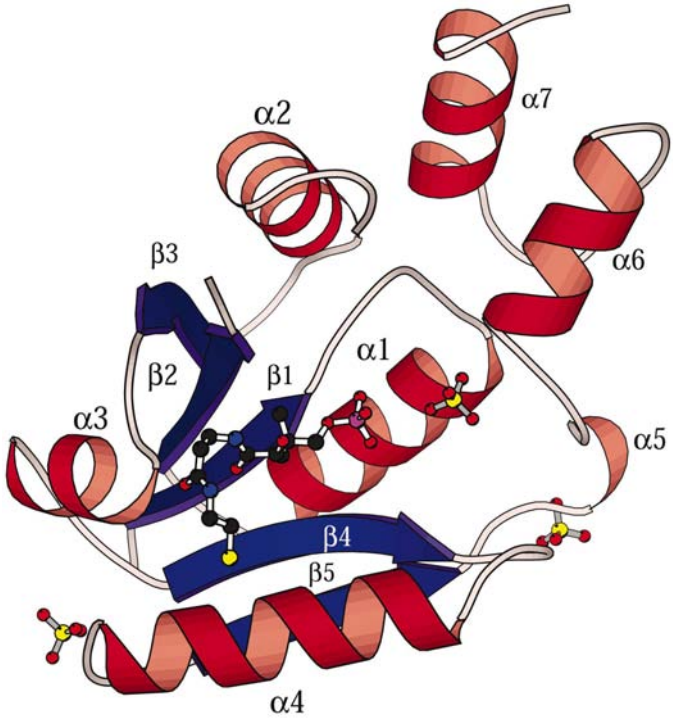


**Figure 2**
Ribbon diagram of the PPAT protomer. $\alpha$-Helices are depicted by red helical ribbons and $\beta$-strands by blue arrows. The substrate, Ppant and three sulfate anions are shown in ball-and-stick representation. The colours of the atoms are the same as in Fig. 1. This figure was produced with *MOLSCRIPT* (Kraulis, 1991).

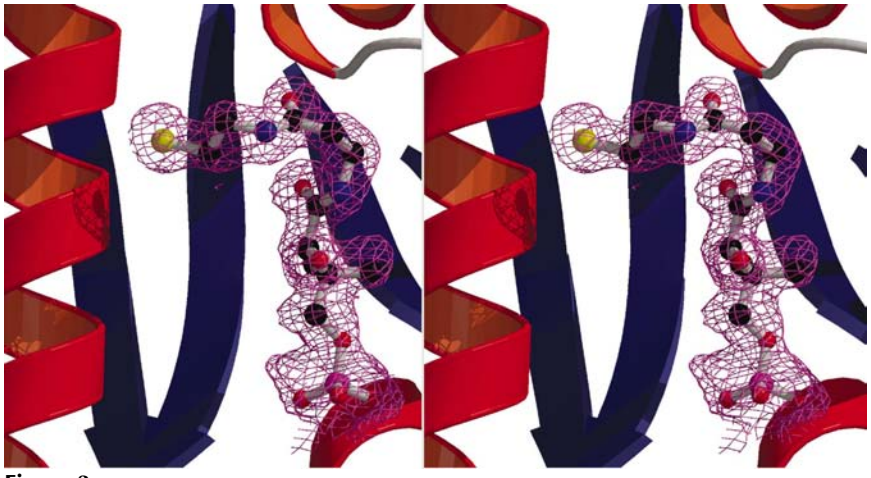

**Figure 3**
Stereoview of a $\sigma_A$-weighted $F_o - F_c$ omit electron-density map (2.5$\sigma$) covering the bound Ppant. Ppant is drawn in ball-and-stick representation. This figure was prepared with *BOBSCRIPT* and *Raster3D* (Kraulis, 1991; Merritt & Bacon, 1997).

The active site of *Tt* PPAT is located on a wide groove in the centre of each protomer which is easily accessible from a central channel. The residues from $\alpha$6 in a neighbouring subunit related by the triad axis complement the substrate-binding site. The flexible substrate Ppant binds to the enzyme in a bent conformation (Figs. 3 and 4). The terminal SH group of Ppant is inserted into a hydrophobic groove formed by Met102, Leu105 and Leu109 in the main protomer and by Met131 and Ile135 from $\alpha$6 of the neighbouring subunit. The side chain of Glu134 in $\alpha$6 forms a hydrogen bond with the amide group of the pantetheine arm. A hydrogen bond between the amide of Leu74 and the carboxylic O atom at the elbow of the pantetheine arm stabilizes the bent conformation. Two Ppant methyl groups are stabilized by hydrophobic interactions with Pro6, Leu35, Phe70 and Leu74. The side chain and the amide group of the conserved Ser8 as well as the ordered water molecule form hydrogen bonds to a non-esterified O atom on the 4′-phosphate of Ppant, which seems to be the nucleophilic atom in the in-line displacement reaction. The Lys88 and Glu99 side chains may be oriented to participate in the nucleophilic reaction (Fig. 5). The invariant residue Lys40, corresponding to Lys42 in the *E. coli* PPAT structure, which has been reported to play a crucial role in orienting the nucleophile (Izard, 2002), is not defined as it is in the disordered loop (Fig. 4). In the *E. coli* PPAT–Ppant complex structure the equivalent loop is ill-defined in the unliganded subunit, but is ordered in the liganded subunit because of the hydrogen bonding of Lys42 to the non-nucleophilic phosphate of Ppant (Izard, 2002). The loop in *Tt* PPAT is two residues longer than the equivalent loop 38–46 in *E. coli* PPAT and thus may be flexible even in the presence of the hydrogen bond between Lys40 and the O atom on the 4′-phosphate.

Alternative conformations are observed for the side chains of five residues: Arg56, Val87, His104, Gln108 and Leu119. Three of these residues participate in subunit communication in the twofold-related interaction. In particular, for His104 and Gln108 one of the alternative conformations of the residue on the dyad interface of a subunit forms a hydrogen bond with other residue on the interface of the twofold-related subunit, stabilizing the dyad interface.

### 3.3. Comparison with *E. coli* PPAT-bound Ppant

Superpositions of the *Tt* PPAT protomer onto ligand-free and ligand-bound protomers of *E. coli* PPAT show overall root-mean-square deviations (r.m.s.d.) for the 151 equivalent C$^\alpha$ positions (except for the flexible loop 37–44) of 0.93 and 1.02 Å,

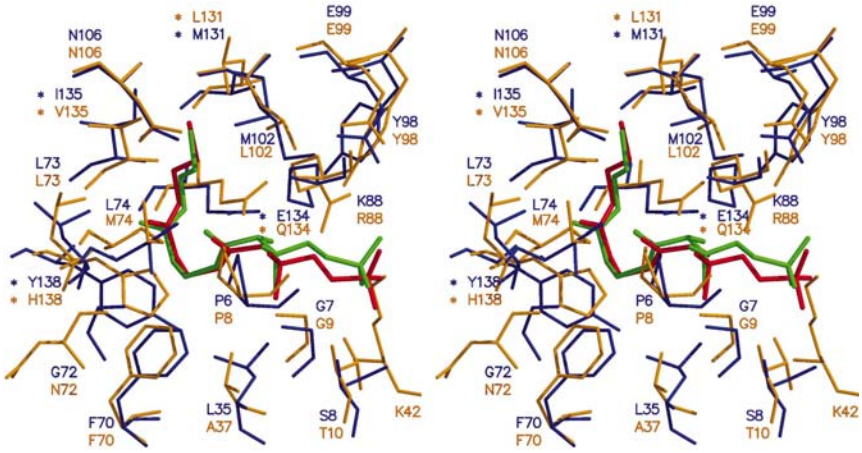


**Figure 4**
Stereo drawing (Bacon & Anderson, 1988; Kraulis, 1991; Merritt & Murphy, 1994) of Ppant bound to *Tt* PPAT and superimposed *E. coli* PPAT. *Tt* PPAT residues are shown in blue and labelled in the same colour, while *E. coli* PPAT residues are in orange and labelled in the same colour. Ppant from *Tt* PPAT is shown in red, while Ppant from *E. coli* PPAT is in green. * denotes residues from neighbouring subunits.

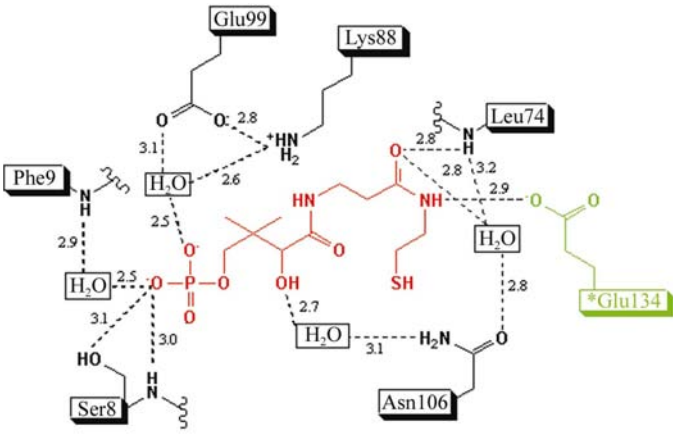


**Figure 5**
Schematic representation of hydrogen bonding between Ppant and *Tt* PPAT. Ppant is shown in red and residues from a protomer of the PPAT hexamer are shown in black. The residue from the neighbouring subunit related by the triad axis is shown in green. The hydrogen bonds are drawn using dashed lines and the donor-to-acceptor distances (Å) are also indicated.

respectively. A large difference in the backbone conformation is found for the loop formed by residues 90–95. Residues 92–94 are ill-defined in *Tt* PPAT. Fig. 4 shows a comparison of the Ppant bound to *Tt* PPAT and *E. coli* PPAT. In *E. coli* PPAT, the amide group of Thr10, corresponding to Ser8 in *Tt* PPAT, forms a hydrogen bond to the nucleophilic O atom of Ppant. The side chain of Arg88 forms hydrogen bonds to an esterified O atom and a non-esterified O atom of the 4′-phosphate of Ppant in *E. coli* PPAT, whereas the corresponding Lys88 and also Glu99 form a water-mediated hydrogen bond only with the non-esterified O atom of the 4′-phosphate in *Tt* PPAT. Lys42 in *E. coli* PPAT, which is disordered in *Tt* PPAT, also interacts with 4′-phosphate from the opposite side of Arg88 and assists in orienting the nucleophile.

### 3.4. Molecular-assembly form of *Tt* PPAT in solution

As described above, we found a notable difference between *E. coli* PPAT and *Tt* PPAT in substrate recognition: all six subunits of *Tt* PPAT simultaneously bind substrate, in contrast to the binding of only three subunits in the *E. coli* PPAT homohexamer. For *E. coli* PPAT, which has a monomer molecular weight of 17.8 kDa, the average value of its apparent molecular weight has been reported to be 108 000 ± 2000 Da from sedimentation-equilibrium experiments involving analytical ultracentrifugation at protein concentrations between 0.4 and 1.2 mg ml$^{-1}$, although it was reported to be 71 200 Da from gel filtration (Geerlof *et al.*, 1999). This indicates that the protein in solution is a homohexamer as in the crystal.

Accordingly, the oligomeric state of *Tt* PPAT, which has a monomer molecular weight of 17.7 kDa, in solution was also examined using analytical ultracentrifugation. The sedimentation-velocity experiment revealed an apparent single boundary with an $s^0_{20,w}$ value of 6.34 S. The average molecular weight was 67 000 ± 4600 Da based on the sedimentation-equilibrium experiment, indicating that the average oligomer is a 3.8-mer. It is very likely that *Tt* PPAT in solution could be in equilibrium between two trimers and a hexamer, judging from the equilibrium experiment and its X-ray structure. Therefore, we analyzed the sedimentation-equilibrium data of *Tt* PPAT assuming it to be in equilibrium between two trimers and a hexamer. As shown in Fig. 6, the analysis was successfully fitted with an association constant of $9.48 \times 10^3\ M^{-1}$, indicating that the assumption is correct and the association constant of *Tt* PPAT in solution is lower than that of *E. coli* PPAT. This agrees with the fact that the intersubunit interactions in a hexamer of *Tt* PPAT might be expected to make it less stable than that of *E. coli* PPAT, as discussed in the following sections. These results suggest that the trimer of *Tt* PPAT is a physiologically important form.

### 3.5. Thermostability

**3.5.1. Contribution of hydrophobic interactions**. Hydrophobic interactions in the interior of a protein are an important stabilizing factor (Kauzmann, 1959). In experiments using a series of hydrophobic mutants of human lysozyme, Takano and coworkers found a general rule for the relationship between hydrophobic effects and the conformational stability of a protein (Takano *et al.*, 1998). The contribution ($\Delta G$) arising from hydrophobic effects on denaturation of a protein can be expressed using changes in the accessible surface area (ASA) of the non-polar and polar atoms arising from denaturation as follows (Funahashi *et al.*, 1999),

$$\Delta G = \alpha \Delta \mathrm{ASA}_{\text{non-polar}} + \beta \Delta \mathrm{ASA}_{\text{polar}}, \qquad (1)$$

**Table 2**
The contribution of hydrophobic interactions to the conformational stability of *Tt* PPAT and *E. coli* PPAT and of hydrophobic interaction, hydrogen bonds and ion pairs to stability in the intersubunit interactions of both proteins.

ASA values are in Å$^2$, $\Delta G$ values are in kJ mol$^{-1}$. $\Delta\Delta G$ represents the difference in $\Delta G$ between *Tt* PPAT and *E. coli* PPAT. 3 *Tt* PPAT and 3 *E. coli* PPAT denote trimers and 6 *Tt* PPAT and 6 *E. coli* PPAT denote hexamers. The intersubunit interactions were examined between a monomer and a trimer and between a trimer and a hexamer. Difference (trimer − monomer) and Difference (hexamer − trimer) represent the difference between *Tt* PPAT and *E. coli* PPAT in the intersubunit interaction differences between a monomer and trimer or a trimer and hexamer, respectively. A positive value indicates that *Tt* PPAT is more stable than *E. coli* PPAT.

| | Hydrophobicity | | | | Intersubunit | | |
|---|---|---|---|---|---|---|---|
| Protein | ΔASA (C/S) | ΔASA (N/O) | $\Delta G$ | $\Delta\Delta G$ | Hydrophobicity ($\Delta\Delta G$) | Hydrogen bond | Ion pair |
| *Tt* PPAT | 9612 | 4250 | 1656 | 40 | | | |
| *E. coli* PPAT | 9379 | 4142 | 1616 | | | | |
| 3 *Tt* PPAT | 31145 | 13760 | 1788 | 16 | 132 | 6 | 0 |
| 3 *E. coli* PPAT | 30846 | 13474 | 1772 | | 156 | 3 | 0 |
| Difference (trimer − monomer) | | | | | −24 | 3 | |
| 6 *Tt* PPAT | 67569 | 29603 | 1940 | 15 | 152 | 36 | 3 |
| 6 *E. coli* PPAT | 67040 | 29383 | 1925 | | 153 | 42 | 4 |
| Difference (hexamer − trimer) | | | | | −1 | −6 | −1 |

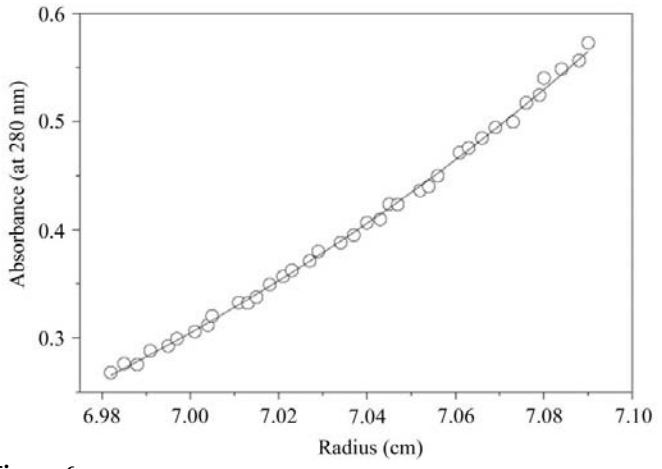


**Figure 6**
Sedimentation-equilibrium analysis of *Tt* PPAT at pH 7.0. The data were analyzed assuming equilibrium between a trimer and a hexamer of *Tt* PPAT. Circles are experimental data and the curve was fitted with an association constant of $9.48 \times 10^3\ M^{-1}$.

where $\Delta ASA_{non\text{-}polar}$ and $\Delta ASA_{polar}$ represent the differences in the ASA value for the non-polar and polar atoms, respectively, in all residues upon denaturation. Using the stability/structure database for a series of mutant human lysozymes, the parameters $\alpha$ and $\beta$ have been determined to be 0.178 and −0.013 kJ mol$^{-1}$ Å$^{-2}$, respectively. For the calculation of ASA, the C and S atoms in residues were assigned as $ASA_{non\text{-}polar}$ and N and O atoms as $ASA_{polar}$ (Tanaka *et al.*, 2001).

We attempted to estimate the contribution of hydrophobic interactions in *Tt* PPAT and *E. coli* PPAT to the stabilization. The ASA values were calculated from the X-ray crystal structures of the two proteins in the native state using the procedure of Connolly (1993). The ASA values in the denatured states were calculated from the extended structures using *Insight II*. The structure of the Ppant monomer of *E. coli* PPAT was used for the calculation. As shown in Table 2, the $\Delta G$ values arising from hydrophobic interactions in *Tt* PPAT are 40, 16 and 15 kJ mol$^{-1}$ per monomer greater than those of *E. coli* PPAT when PPAT is assumed to be a monomer, a trimer and a hexamer in solution, respectively. These data show that hydrophobic interactions are stronger in *Tt* PPAT than in *E. coli* PPAT, contributing to the higher stability of *Tt* PPAT, especially in the monomeric state. The difference in hydrophobic interactions betweeen the monomer and trimer was 24 kJ mol$^{-1}$ lower than that for *E. coli* PPAT (Table 2). The differences in hydrophobic interactions between the trimer and hexamer were similar for both proteins (Table 2). This suggests that the hydrophobic effect from the intersubunit interactions of oligomers does not contribute to the higher stability of *Tt* PPAT, although oligomerization has been reported to be one strategy used to stabilize proteins in thermophilic organisms (Ogasawara *et al.*, 2003).

**3.5.2. Contribution of ion pairs**. Ion-pair networks on the protein surface are usually assumed to be stabilizing (Hening *et al.*, 1995; Yip *et al.*, 1995; Pappenberger *et al.*, 1997). The number of ion pairs formed within 5 Å is 0.14 and 0.13 (per residue) for *Tt* PPAT and *E. coli* PPAT, respectively. In *Tt* PPAT, three residues are involved in the formation of three intramolecular ion pairs (between subunits related by the dyad; Table 2). In *E. coli* PPAT, four intramolecular ion pairs involving four residues are formed (Table 2). Two of these are between subunits related to the dyad and the other two are between subunits corresponding to the yellow and the green subunits in Fig. 1. A remarkable increase in the number of ion pairs in *Tt* PPAT was not observed compared with that in *E. coli* PPAT.

**3.5.3. Contribution of hydrogen bonds**. Hydrogen bonds are ubiquitous in proteins and their contribution to conformational stability is of fundamental importance, as are hydrophobic interactions. Recently, the net contribution of an intramolecular hydrogen bond has been estimated to be 8.5 kJ mol$^{-1}$ for a 3 Å hydrogen bond; this was determined using a series of hydrogen-bond mutants of human lysozyme (Takano *et al.*, 1999). The average number of hydrogen bonds per residue in *Tt* PPAT and *E. coli* PPAT is 1.07 and 1.03, respectively. The total number of hydrogen bonds in the *Tt* PPAT hexamer (996 bonds in 930 residues) is greater than in the *E. coli* PPAT hexamer (948 bonds in 924 residues). Of these hydrogen bonds, there are 36 and 42 intersubunit hydrogen bonds in the *Tt* PPAT hexamer and *E. coli* PPAT hexamer, respectively (Table 2). In particular, the difference in the number of intersubunit hydrogen bonds in *E. coli* PPAT

between the trimer and hexamer was greater by six than that of *Tt* PPAT (Table 2). The increase in the total number of hydrogen bonds might contribute to the higher stability of the *Tt* PPAT monomer compared with the *E. coli* PPAT. However, the subunit interaction between the trimer and hexamer of *E. coli* PPAT is more stable compared with that of *Tt* PPAT because the hydrogen bonds are stronger, although the hydrophobic interaction is comparable.

**3.5.4. Entropic effects**. Important stabilizing factors include entropic effects. When the conformational entropy of a protein is decreased in the denatured state owing to substitutions or deletion, the protein may be stabilized. The entropic effects of denaturation arising from the side chains of the amino-acid residues can be calculated from their amino-acid compositions using the thermodynamic parameters proposed by Oobatake & Ooi (1993); the denaturation entropies for *Tt* PPAT and *E. coli* PPAT were calculated to be 0.28 and 0.56 kJ $mol^{-1}$ $K^{-1}$, respectively. This indicates that the entropic effects owing to the features of the residues remarkably contribute to the higher stability of the thermophilic protein. On the other hand, entropic effects are caused by introduction of disulfide bonds, the side chains, including substitution of Pro residues and the shortening of polypeptides. Both *Tt* PPAT and *E. coli* PPAT contain no Cys residues and therefore no disulfide bonds. The number of Pro residues is six and seven in *Tt* PPAT and *E. coli* PPAT, respectively, suggesting that there is a slight difference in stability owing to the Pro content.

**3.5.5. Stability of the intersubunit interactions between trimer and hexamer**. The intersubunit interactions of *Tt* PPAT across the dyad axis of the oligomer were in equilibrium between the trimer and hexamer and its association constant seemed to be lower than that of *E. coli* PPAT. We have already discussed the difference in the stabilizing forces in the intersubunit interaction for both X-ray structures. The surface areas of the boundary of *Tt* PPAT and *E. coli* PPAT were 1159 and 1224 Å per monomer, respectively. The increase in *E. coli* PPAT was because of the increase in polar atoms. Therefore, the number of hydrogen bonds and ionic bonds in *Tt* PPAT was lower. However, the hydrophobic interaction of the interaction surface of *Tt* PPAT was comparable to its counterpart. As a result, the increase in the number of hydrogen bonds and ionic bonds in *E. coli* PPAT might contribute to the larger difference in intersubunit interactions between the trimer and hexamer, which agrees with analytical ultracentrifugation results. These results suggest that the hexameric form of *Tt* PPAT is not a physiologically important form.

## 4. Conclusion

The overall structure of *Tt* PPAT–Ppant, including the active site (Fig. 5), is similar to that of *E. coli* PPAT–Ppant (Izard, 2002), suggesting similarity in the function of both proteins. Therefore, as in *Tt* PPAT, it seems that the 4′-phosphate of Ppant undergoes nucleophilic attack on the $\alpha$-phosphate of the nucleotide *via* an in-line displacement mechanism.

The enzyme binds the substrate at both a main binding subunit and a neighbouring subunit related to the triad axis. This indicates that PPAT needs to form at least a trimer in order to achieve functionality. The most remarkable difference between *Tt* PPAT and *E. coli* PPAT was in the manner of the substrate binding; within the PPAT hexamer all subunits in *Tt* PPAT are bound to Ppant molecules, whereas in *E. coli* PPAT the subunits of only one trimer bind to the ligands.

The thermostabilization mechanism of the structure of *Tt* PPAT was examined and compared with that of *E. coli* PPAT. The higher stability of the monomeric structure of *Tt* PPAT arises from a combination of hydrophobic effects, hydrogen bonds and entropic effects, but not from salt bridges. The subunit interaction does not contribute to the higher stability of *Tt* PPAT, indicating that high stability of each subunit is essential for the thermostability of *Tt* PPAT.

We are grateful to Naoko Takahashi, Mayumi Sugahara and Koji Takio for functional analysis of PPAT and to Takashi Matsumoto for crystallization. This work was supported by National Project on Protein Structural and Functional Analysis funded by MEXT of Japan (Project No. TT0265/HTPF00113).

## References

Bacon, D. J. & Anderson, W. F. (1988). *J. Mol. Graph.* **6**, 219–220.
Bork, P., Holm, L., Koonin, E. V. & Sander, C. (1995). *Proteins Struct. Funct. Genet.* **22**, 259–266.
Brünger, A. T., Adams, P. D., Clore, G. M., DeLano, W. L., Gros, P., Grosse-Kunstleve, R. W., Jiang, J.-S., Kuszewski, J., Nilges, M., Pannu, N. S., Read, R. J., Rice, L. M., Simonson, T. & Warren, G. L. (1998). *Acta Cryst.* D**54**, 905–921.
Brünger, A. T., Kuriyan, J. & Karplus, M. (1987). *Science*, **235**, 458–460.
Connolly, M. L. (1993). *J. Mol. Graph.* **11**, 139–141.
Funahashi, J., Takano, K., Yamagata, Y. & Yutani, K. (1999). *Protein Eng.* **12**, 841–850.
Geerlof, A., Lewendon, A. & Shaw, W. V. (1999). *J. Biol. Chem.* **274**, 27105–27111.
Gerdes, S. Y., Scholle, M. D., D'Souza, M., Bernal, A., Baev, M. V., Farrell, M., Kurnasov, O. V., Daugherty, M. D., Mseeh, F., Polanuyer, B. M., Campbell, J. W., Anantha, S., Shatalin, K. Y., Choedhury, S. A., Fonstein, M. Y. & Osterman, A. L. (2002). *J. Bacteriol.* **184.** 4555–4572.
Halvorsen, O. & Skrede, S. (1982). *Eur. J. Biochem.* **124**, 211–215.
Hening, M., Darimont, B., Sterner, R., Kirschner, K. & Jansonius, J. N. (1995). *Structure*, **3**, 1295–1306.
Izard, T. (2002). *J. Mol. Biol.* **315**, 487–495.
Izard, T. & Geerlof, A. (1999). *EMBO J.* **18**, 2021–2030.
Jackowski, S. & Rock, C. O. (1984). *J. Bacteriol.* **158**, 115–120.
Kauzmann, W. (1959). *Adv. Protein Chem.* **14**, 1–63.
Kraulis, P. J. (1991). *J. Appl. Cryst.* **24**, 946–950.
Matthews, B. W. (1968). *J. Mol. Biol.* **33**, 491–497.
Merritt, E. A. & Bacon, D. J. (1997). *Methods Enzymol.* **277**, 505–524.
Merritt, E. A. & Murphy, M. E. P. (1994). *Acta Cryst.* D**50**, 869–873.
Ogasawara, K., Ishida, M. & Yutani, K. (2003). *J. Biol. Chem.* **14**, 8922–8928.
Oobatake, M. & Ooi, T. (1993). *Prog. Biophys. Mol. Biol.* **59**, 237–284.
Otwinowski, Z. & Minor, W. (1997). *Methods Enzymol.* **276**, 307–326.
Pappenberger, G., Schurig, H. & Jaenicke, R. (1997). *J. Mol. Biol.* **274**, 676–683.

Robinshaw, J. D. & Neely, J. R. (1985). *Am. J. Physiol.* **248**, E1–E9.
Rossmann, M. G., Lilijas, A., Brändén, C. I. & Banaszak, L. J. (1975). *The Enzymes*, edited by P. D. Boyer, pp. 62–102. New York: Academic Press.
Sugahara, M. & Miyano, M. (2002). *Tanpakushitsu Kakusan Koso*, **47**, 1026–1032.
Takano, K., Yamagata, Y., Funahashi, J., Hiroki, Y., Kuramitsu, S. & Yutani, K. (1999). *Biochemistry*, **38**, 12698–12708.
Takano, K., Yamagata, Y. & Yutani, K. (1998). *J. Mol. Biol.* **280**, 749–761.
Tanaka, H., Chinami, M., Mizushima, T., Ogasawara, K., Ota, M., Tsukihara, T. & Yutani, K. (2001). *J. Biochem.* **130**, 107–118.
Yip, K. S. P., Stillman, T. J., Britton, K. L., Artymiuk, P. J., Baker, P. J., Sedelnikova, S. E., Engel, P. C., Pasquo, A., Chiaraluce, R. & Consalvi, V. (1995). *Structure*, **3**, 1147–1158.